applied sciences

MDPI

Article

Spatial-Temporal Self-Focusing of Partially Coherent Pulsed Beams in Dispersive Medium

Zhiguo Zhao *, Chaoliang Ding, Yongtao Zhang and Liuzhan Pan

College of Physics and Electronic Information & Henan Key Laboratory of Electromagnetic Transformation and Detection, Luoyang Normal University, Luoyang 471934, China

* Correspondence: zhiguozhao@lynu.edu.cn; Tel.: +86-379-6861-8310

Received: 14 August 2019; Accepted: 24 August 2019; Published: 3 September 2019

Featured Application: The results obtained in this paper will provide a scientific reference for the applications of ultra-short pulses in laser micromachining.

Abstract: Partially coherent pulsed beams have many applications in pulse shaping, fiber optics, ghost imaging, etc. In this paper, a novel class of partially coherent pulsed (PCP) sources with circular spatial coherence distribution and sinc temporal coherence distribution is introduced. The analytic formula for the spatial-temporal intensity of pulsed beams generated by this kind of source in dispersive media is derived. The evolution behavior of spatial-temporal intensity of the pulsed beams in water and air is investigated, respectively. It is found that the pulsed beams exhibit spatial-temporal self-focusing behavior upon propagation. Furthermore, a physical interpretation of the spatial-temporal self-focusing phenomenon is given. This is a phenomenon of optical nonlinearity, which may have potential application in laser micromachining and laser filamentation.

Keywords: coherence and statistical optics; propagation; partially coherent; pulses

1. Introduction

As we all know, the coherence properties of a light source have a marked impact on the characteristics of the propagated field, especially on the intensity profile. Hence, it is a possible way to modulate the beam shape by regulating the coherence of the source [1–7]. In the past few decades, extensive work have been done to control the coherence distribution of light sources in order to obtain desired far-field intensity profile or extraordinary propagation behaviors [8–32], such as self-splitting, self-focusing, self-steering, and flat-topping, ring-shaped, rectangular, gridded, dark-hollow, or cusped intensity profiles, which have many applications in remote sensing [33], imaging [34], optical trapping and optical communications [35].

In 2017, a new class of partially coherent light sources with circular coherence was introduced [36] and synthesized through a time multiplexing approach [37]. Then, Hyde IV et al. proposed another alternative approach for synthesizing this class of sources [38]. The self-focusing propagation phenomenon of this class of sources was also founded, whose propagation properties through oceanic turbulence is also being explored [39]. All the above-mentioned references are confined to stationary optical fields or beams.

On the other hand, random optical pulses with partial temporal or spectral coherence represent more widespread partially coherent light fields, which have many applications in pulse shaping, fiber optics, ghost imaging etc. [40–42]. In practice, many real sources, such as excimer lasers, free-electron lasers, or random lasers generate partially coherent pulse trains [43]. Usually, the Gaussian Schell-model (GSM) pulses with Gaussian correlation function are used to describe the partially coherent pulsed (PCP) field, which is called partially coherent GSM pulsed beams [44–46], whose propagation properties

are investigated in detailed [47–55]. In 2013, the non-uniformly PCP source with non-conventional correlation functions are introduced by Lajunen and Saastamoinen [56]. The propagation properties of various non-uniformly PCP source exhibit many interesting behaviors, such as pulse self-splitting, self-focusing and adjustable pulse profile [57–61].

In this paper, we present a novel class of spatially and temporally PCP source with circular spatial coherence distribution and sinc temporal coherence distribution. The propagation properties of pulsed beams generated by this source in two common dispersive media, i.e., water and air are investigated. It is found that, the pulsed beams exhibit spatial-temporal self-focusing behavior upon propagation in water or air. The condition that the self-focusing takes place at spatial domain and temporal domain simultaneously is acquired. In Section 2, based on the optical coherence theory of non-stationary field, we obtain the spatial-temporal intensity distribution of the proposed PCP beams. In Section 3, we give numerical calculations, and present the spatial-temporal self-focusing behavior of the pulsed beams in water and air, respectively. In addition, a physical interpretation of the spatial-temporal self-focusing phenomenon is presented. In Section 4, we summarize the results.

2. Theory

Consider a statistically PCP source located in the plane $z = 0$, radiating a beam-like field that propagates into the positive half-space $z > 0$. The statistical properties of the 2D source at points $\boldsymbol{\rho}_1 = (x_1', y_1')$ and $\boldsymbol{\rho}_2 = (x_2', y_2')$, at different instant time t_{10} and t_{20}, can be characterized by the mutual coherent function (MCF), which is defined as a two-point two-time correlation function without spatiotemporal coupling:

$$\Gamma_0(\boldsymbol{\rho}_1, t_{10}; \boldsymbol{\rho}_2, t_{20}) = R(\boldsymbol{\rho}_1, \boldsymbol{\rho}_2) T(t_{10}, t_{20}) \tag{1}$$

where

$$R(\boldsymbol{\rho}_1, \boldsymbol{\rho}_2) = \exp\left(-\frac{\rho_1^2 + \rho_2^2}{2w_0^2}\right) \mathrm{sinc}\left(-\frac{\rho_2^2 - \rho_1^2}{\sigma^2}\right) \tag{2}$$

$$T(t_{10}, t_{20}) = \exp\left(-\frac{t_{10}^2 + t_{20}^2}{2T_0^2}\right) \mathrm{sinc}\left(-\frac{t_{20}^2 - t_{10}^2}{T_c^2}\right) \exp\left[-i\omega_0\left(t_{20} - t_{10}\right)\right] \tag{3}$$

where $\mathrm{sinc}x = \sin\pi x/\pi x$ and ω_0 is the carrier frequency of pulsed beams. w_0 and σ denotes beam width and spatial coherent parameter, respectively. T_0 and T_c represent pulse duration and temporal coherent length, respectively. The beams generated by this kind of pulsed source expressed by Equation (1) are regarded as the spatially and temporally PCP beams with circular spatial and sinc temporal coherence distribution. The spatial part of mutual coherent function Equation (1) is the same as that in reference [39], which has a circular coherence distribution. Equation (1) can be also written as:

$$\Gamma_0(\boldsymbol{\rho}_1, t_{10}; \boldsymbol{\rho}_2, t_{20}) = \int_{-\infty}^{\infty}\int_{-\infty}^{\infty} p_R(v_1) p_T(v_2) H^*(\boldsymbol{\rho}_1, t_{10}, v_1, v_2) H(\boldsymbol{\rho}_2, t_{20}, v_1, v_2) dv_1 dv_2 \tag{4}$$

where

$$p_R(v_1) = \sigma^2 \mathrm{rect}(\sigma^2 v_1) \tag{5}$$

$$p_T(v_2) = T_c^2 \mathrm{rect}(T_c^2 v_2) \tag{6}$$

$$H(\boldsymbol{\rho}, t_0; v_1, v_2) = H_R(\boldsymbol{\rho}, v_1) H_T(t_0, v_2) \tag{7}$$

$$H_R(\boldsymbol{\rho}, v_1) = \exp\left(-\frac{\rho^2}{2w_0^2}\right) \exp\left(-2\pi i v_1 \rho^2\right) \tag{8}$$

$$H_T(t_0, v_2) = \exp\left(-\frac{t_0^2}{2T_0^2}\right) \exp\left(-2\pi i v_2 t_0^2\right) \exp(-i\omega_0 t_0) \tag{9}$$

where $p_{\mathrm{R}}(v_1)$ and $p_{\mathrm{T}}(v_2)$ are rect weight functions of $H(\cdot)$. In the plane $z > 0$, by means of the extended Huygens-Fresnel integral with paraxial approximation, the propagation properties of PCP beams with circular spatial and sinc temporal coherence distribution in dispersive medium in spatiotemporal domain can be characterized by the following integral formula [1,62]:

$$\begin{aligned}\Gamma(\boldsymbol{r}_1,\boldsymbol{r}_2,t_1,t_2,z) &= \left(\tfrac{k}{2\pi z}\right)^2 \tfrac{\omega_0}{2\pi a}\int\int\int\int_{-\infty}^{\infty}\Gamma_0(\boldsymbol{\rho}_1,t_{10};\boldsymbol{\rho}_2,t_{20})\\ &\times\exp\left[-ik\tfrac{(\boldsymbol{r}_1-\boldsymbol{\rho}_1)^2-(\boldsymbol{r}_2-\boldsymbol{\rho}_2)^2}{2z}\right]d^2\boldsymbol{\rho}_1 d^2\boldsymbol{\rho}_2\\ &\times\exp\left[-i\omega_0\tfrac{(t_1-t_{10})^2-(t_2-t_{20})^2}{2a}\right]dt_{10}dt_{20},\end{aligned} \tag{10}$$

where $k = n(\omega)/c$ denotes the wave number, in which $n(\omega)$ is refractive index of medium and c is the speed of light in vacuum. In this paper, we assume that the medium is a linear dispersive medium whose refractive index is given by $n(\omega) = n_{\mathrm{a}}\omega + n_{\mathrm{b}}$, where n_{a} and n_{b} are constants. And $a = \omega_0\beta_2 z$, with β_2 representing the group velocity dispersion, which is related to n_{a} by $\beta_2 = n_{\mathrm{a}}/c$. And $n_{\mathrm{b}} = 2\beta_2\omega_0 c - c/v_{\mathrm{g}}$, where v_{g} is the group velocity of the pulse [63]. Here, the time coordinate is a retarded time, which is calculated in a frame moving with group velocity of the pulses.

On substituting Equations (4) and (7) into (10), by interchanging the orders of the integrals, we can derive the formula:

$$\Gamma(\boldsymbol{r}_1,\boldsymbol{r}_2,t_1,t_2,z) = \int_{-\infty}^{\infty}\int_{-\infty}^{\infty} p_R(v_1)p_T(v_2)H^*(\boldsymbol{r}_1,t_1,v_1,v_2,z)H(\boldsymbol{r}_2,t_2,v_1,v_2,z)dv_1dv_2 \tag{11}$$

where

$$H^*(\boldsymbol{r}_1,t_1,v_1,v_2,z)H(\boldsymbol{r}_2,t_2,v_1,v_2,z) = H_R^*(\boldsymbol{r}_1,v_1,z)H_R(\boldsymbol{r}_2,v_1,z)H_T^*(t_1,v_2,z)H_T(t_2,v_2,z) \tag{12}$$

and

$$\begin{aligned}H_R^*(\boldsymbol{r}_1,v_1,z)H_R(\boldsymbol{r}_2,v_1,z) &= \left(\tfrac{k}{2\pi z}\right)^2\int\int_{-\infty}^{\infty}H_R^*(\boldsymbol{\rho}_1,v_1)H_R(\boldsymbol{\rho}_2,v_1)\\ &\times\exp\left[-ik\tfrac{(\boldsymbol{r}_1-\boldsymbol{\rho}_1)^2-(\boldsymbol{r}_2-\boldsymbol{\rho}_2)^2}{2z}\right]d^2\boldsymbol{\rho}_1 d^2\boldsymbol{\rho}_2,\end{aligned} \tag{13}$$

and

$$\begin{aligned}H_T^*(t_1,v_2,z)H_T(t_2,v_2,z) &= \tfrac{\omega_0}{2\pi a}\int\int_{-\infty}^{\infty}H_T^*(t_{10},v_2)H_T(t_{20},v_2)\\ &\times\exp\left[-i\omega_0\tfrac{(t_1-t_{10})^2-(t_2-t_{20})^2}{2a}\right]dt_{10}dt_{20}.\end{aligned} \tag{14}$$

By inserting Equations (8) and (9) into (13) and (14), respectively, after a tedious integral calculation, one can obtain:

$$\begin{aligned}H_R^*(\boldsymbol{r}_1,v_1,z)H_R(\boldsymbol{r}_2,v_1,z) &= \tfrac{w_0^2}{w^2(z)}\exp\left[\tfrac{ik}{2z}\left(r_2^2-r_1^2\right)\right]\exp\left[-\tfrac{k^2w_0^2}{4z^2}\left(\boldsymbol{r}_2-\boldsymbol{r}_1\right)^2\right]\\ &\times\exp\left\{-\tfrac{1}{w^2(z)}\left[\tfrac{\boldsymbol{r}_1+\boldsymbol{r}_2}{2}+\tfrac{ikw_0^2}{2z}\left(1-\tfrac{4\pi v_1 z}{k}\right)\left(\boldsymbol{r}_2-\boldsymbol{r}_1\right)\right]^2\right\},\end{aligned} \tag{15}$$

and

$$\begin{aligned}H_T^*(t_1,v_2,z)H_T(t_2,v_2,z) &= \tfrac{T_0}{T(z)}\exp\left[\tfrac{i}{2\beta_2 z}\left(t_2^2-t_1^2\right)\right]\exp\left[-\tfrac{T_0^2}{4\beta_2^2z^2}\left(t_2-t_1\right)^2\right]\\ &\times\exp\left\{-\tfrac{1}{T^2(z)}\left[\tfrac{t_1+t_2}{2}+\tfrac{iT_0^2}{2\beta_2 z}(1-4\pi v_2\beta_2 z)\left(t_2-t_1\right)\right]^2\right\},\end{aligned} \tag{16}$$

where

$$w^2(z) = w_0^2\left(1-\frac{4\pi v_1 z}{k}\right)+\left(\frac{z}{kw_0}\right)^2 \tag{17}$$

$$T^2(z) = T_0^2(1 - 4\pi v_2\beta_2 z)^2 + \left(\frac{\beta_2 z}{T_0}\right)^2 \tag{18}$$

If we let $\boldsymbol{r}_1 = \boldsymbol{r}_2 = \boldsymbol{r}$ and $t_1 = t_2 = t$ in Equations (15) and (16), respectively, we can obtain:

$$\left|H_R(\boldsymbol{r}, v_1, z)\right|^2 = \frac{w_0^2}{w^2(z)} \exp\left[-\frac{\boldsymbol{r}^2}{w^2(z)}\right] \tag{19}$$

$$\left|H_T(t, v_2, z)\right|^2 = \frac{T_0}{T(z)} \exp\left[-\frac{t^2}{T^2(z)}\right]. \tag{20}$$

According to Equation (11), we can get spatial-temporal intensity as:

$$I(\boldsymbol{r}, t; \boldsymbol{r}, t, z) = \int_{-\infty}^{\infty}\int_{-\infty}^{\infty} p_R(v_1)p_T(v_2)\left|H_R(\boldsymbol{r}, v_1, z)\right|^2\left|H_T(t, v_2, z)\right|^2 dv_1 dv_2 \tag{21}$$

Equation (21) is the main formula derived in this paper, which is used to investigate the spatial-temporal intensity evolution of the PCP beams in dispersive medium.

If we choose the Gaussian weight function to replace Equations (5) and (6), respectively, i.e.,

$$p'_R(v_1) = \frac{\sigma^2}{\sqrt{\pi}} \exp\left(-\sigma^4 v_1^2\right) \tag{22}$$

$$p'_T(v_2) = \frac{T_c^2}{\sqrt{\pi}} \exp\left(-T_c^4 v_2^2\right) \tag{23}$$

and considering Equations (4), (7)–(9), we can obtain:

$$\Gamma'_0(\boldsymbol{\rho}_1, t_{10}; \boldsymbol{\rho}_2, t_{20}) = R'(\boldsymbol{\rho}_1, \boldsymbol{\rho}_2)T'(t_{10}, t_{20}) \tag{24}$$

where

$$R'\left(\boldsymbol{\rho}_1, \boldsymbol{\rho}_2\right) = \exp\left(-\frac{\rho_1^2 + \rho_2^2}{2w_0^2}\right)\exp\left[-\frac{\left(\rho_2^2 - \rho_1^2\right)^2}{\sigma_c^4}\right] \tag{25}$$

$$T'(t_{10}, t_{20}) = \exp\left(-\frac{t_{10}^2 + t_{20}^2}{2T_0^2}\right)\exp\left[-\frac{\left(t_{20}^2 - t_{10}^2\right)^2}{T_c'^4}\right]\exp\left[-i\omega_0\left(t_{20} - t_{10}\right)\right] \tag{26}$$

where $\sigma_c = \sigma/\sqrt{\pi}$ and $T'_c = T_c/\sqrt{\pi}$. As can be seen from Equations (25) and (26), the spatial part and temporal parts of HCFs have non-uniform coherence distribution. And spatial and temporal parts of MCFs are the same as those in Ref. [64] and Ref. [56], respectively.

3. Spatial-Temporal Self-Focusing of PCP Beams in Dispersive Medium

In this section, the propagation properties of the proposed PCP beams in dispersive medium are investigated. Water and air are chosen as two common examples of dispersive medium. The evolution behavior of the proposed PCP beams upon propagation is explored by detailed numerical simulations. In the following calculation, the pulses and medium parameters are chosen to be w_0 = 1 cm, σ = 1 cm, T_0 = 6 ps, T_c = 4 ps, ω_0 = 2.355 rad/fs and β_2 = 24.88 ps^2 km^{-1} unless different values are specified.

3.1. Water Case

Figures 1a–c and 2a–c give the evolution of normalized spatial-temporal intensity of PCP beams with different values of time t in the x-z plane, while the corresponding on-axis profile are given in Figures 1d and 2d, respectively. Figure 1 is the case of rect weight function case, which corresponds to the pulses with circular spatial and sinc temporal coherence distribution. Figure 2 is the case of

Gaussian weight function, which corresponds to pulses with non-uniform coherence distribution. We choose water as the dispersive medium with refractive index $n_g = c/v_g = 1.3425$ (water, 20 °C). As can be seen, there is an intensity maximum upon propagation, i.e., the spatial-temporal self-focusing takes place upon the water medium propagation. In addition, detection time t has an important effect on the intensity distribution of pulsed beams. With increasing time t, the value of the peak intensity becomes small and the focal spot shifts slightly far from the source plane. Physically, the spatial-temporal intensities of the pulsed beams depend on the spatial positions and detection time t, respectively. As can be seen from Equation (20), detection time t has a close relationship with pulse duration $T(z)$. Furthermore, as shown in Equation (18), $T(z)$ is dependent of z. That is why the detection time affects intensity peak and position of peak intensity.

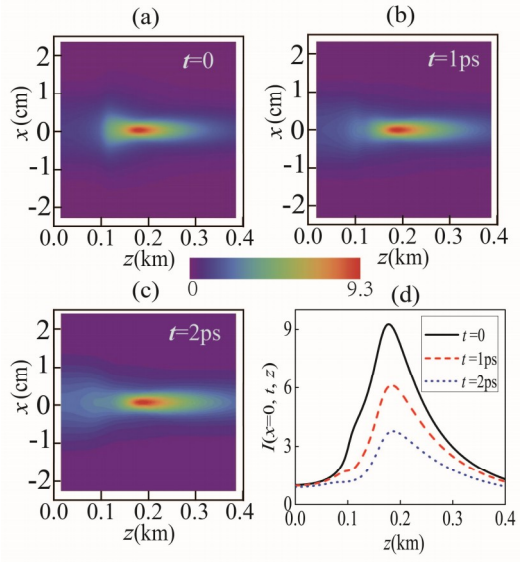

Figure 1. Evolution of normalized spatial-temporal intensity $I(x, t, z)$ of PCP beams with rect weight function with different values of time t: (**a**) $t = 0$, (**b**) $t = 1$ ps and (**c**) $t = 2$ ps in the x-z plane. (**d**) On-axis normalized spatial-temporal intensity versus propagation distance z.

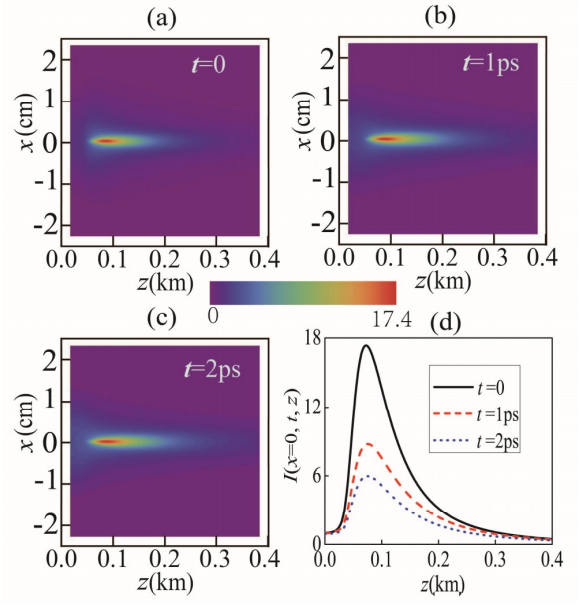

Figure 2. Evolution of normalized spatial-temporal intensity $I(x, t, z)$ of PCP beams with Gaussian weight function with different values of time t: (**a**) $t = 0$, (**b**) $t = 1$ ps and (**c**) $t = 2$ ps in the x-z plane. (**d**) On-axis normalized spatial-temporal intensity versus propagation distance z.

Figures 3a–c and 4a–c give the evolution of normalized spatial-temporal intensity of PCP beams with different values of x in the t-z plane, while the corresponding on-axis and off-axis profile are given in Figures 3d and 4d, respectively. Figure 3 is the case of rect weight function, while Figure 4 is the case of Gaussian weight function. As can be seen, the spatial-temporal self-focusing occurs not only at on-axis ($x = 0$) but also the off-axis ($x \neq 0$). And, with increasing x, the focal spot shifts slightly towards the source plane. Physically, the spatial-temporal intensities of the pulsed beams depend on the spatial positions and detection time t, respectively. When detection time t is fixed, the intensity distribution has a marked impact on position coordinates, which can be seen easily from Equations (17) and (19).

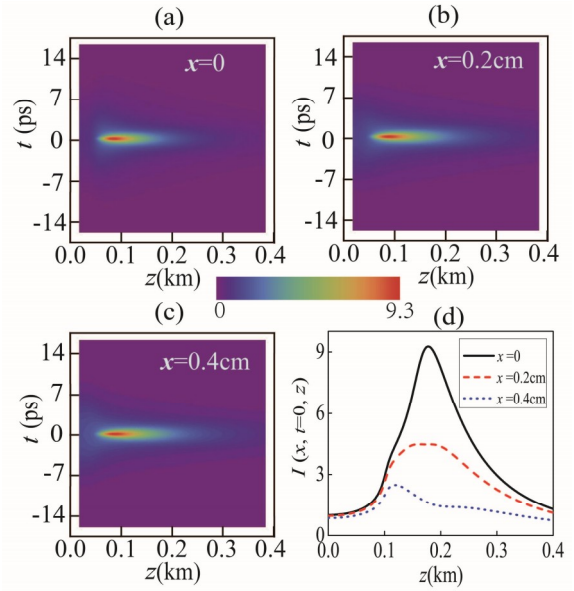

Figure 3. Evolution of normalized spatial-temporal intensity $I(x, t, z)$ of PCP beams with rect weight function with different values of x: (**a**) $x = 0$, (**b**) $x = 0.2$ cm and (**c**) $x = 0.4$ cm in the t-z plane. (**d**) Normalized spatial-temporal intensity versus propagation distance z with $t = 0$.

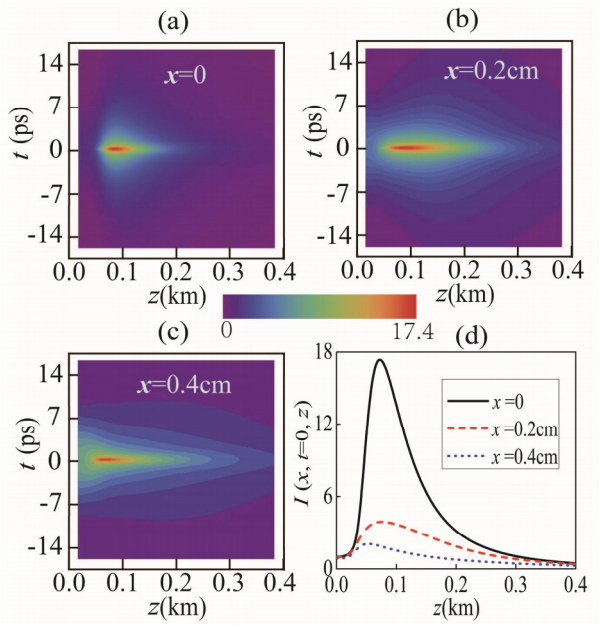

Figure 4. Evolution of normalized spatial-temporal intensity $I(x, t, z)$ of PCP beams with Gaussian weight function with different values of x: (**a**) $x = 0$, (**b**) $x = 0.2$ cm and (**c**) $x = 0.4$ cm in the t-z plane. (**d**) Normalized spatial-temporal intensity versus propagation distance z with $t = 0$.

Figures 5 and 6 give the contour graph of normalized spatial-temporal intensity distribution of PCP beams at the z plane with different values of propagation distance z. Figure 5 is the case of rect weight function, while Figure 6 is the case of Gaussian weight function. It is shown that at the $z = 0$ plane, the pulse duration and beam spatial width is quite large. With increasing z, the pulses focus first on the temporal dimension, then on the spatial dimension. However, at some critical distance, the pulses focus on temporal dimension and spatial dimension simultaneously (see Figure 5c $z = 0.2$ km and Figure 6c $z = 0.04$ km).

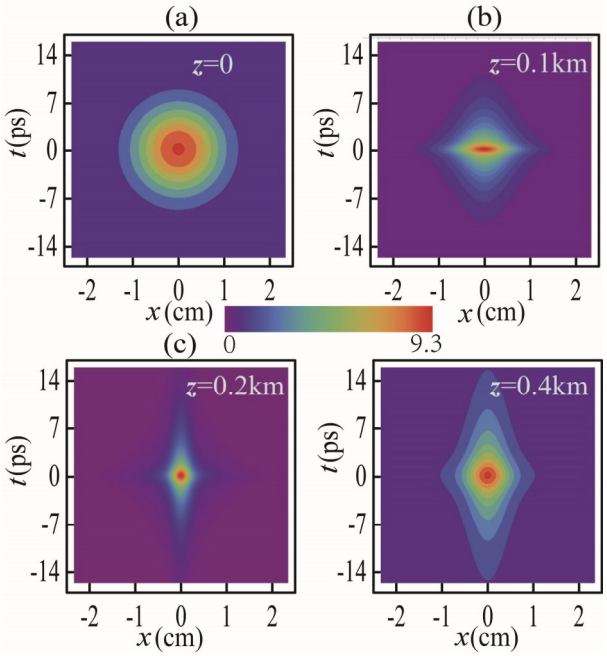

Figure 5. Contour graph of normalized spatial-temporal intensity distribution $I(x, t, z)$ of PCP beams with rect weight function at z plane with different values of z: (**a**) $z = 0$, (**b**) $z = 0.1$ km, (**c**) $z = 0.2$ km and (**d**) $z = 0.4$ km in the x-t plane.

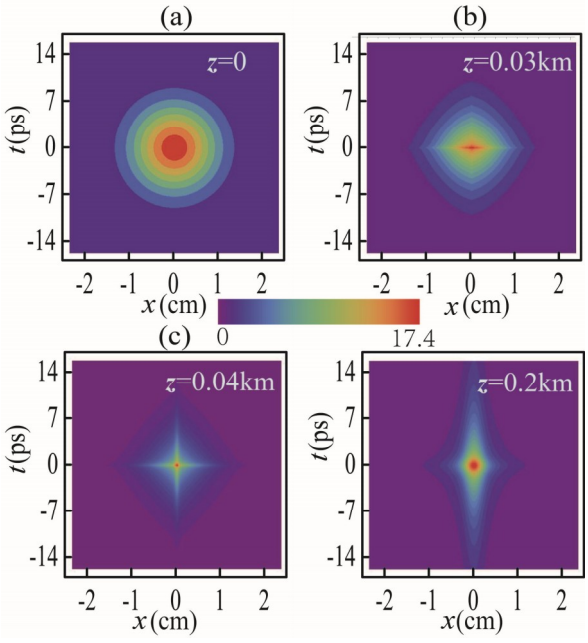

Figure 6. Contour graph of normalized spatial-temporal intensity distribution $I(x, t, z)$ of PCP beams with Gaussian weight function at z plane with different values of z: (**a**) $z = 0$, (**b**) $z = 0.03$ km, (**c**) $z = 0.04$ km and (**d**) $z = 0.2$ km in the x-t plane.

The spatial-temporal self-focusing behavior shown in Figures 5 and 6 can be interpreted as follows. There is some kind of relationship between spatial parameters and temporal parameters, which can be easily seen from the beam spatial width in Equation (17) and pulse duration in Equation (18) of elementary modes of PCP beams; this is because Equations (17) and (18) imply that there are minima for the beam width and pulse duration, respectively. Hence, there are intensity maximum during propagation, when beam widths or pulse durations arrive minima at the same time. More specifically, Equations (17) and (18) can be expanded and re-written as:

$$w^2(z) = a_1 z^2 + b_1 z + c_1 \tag{27}$$

$$T^2(z) = a_2 z^2 + b_2 z + c_2 \tag{28}$$

$$a_1 = \frac{16\pi v_1^2 w_0^4 + 1}{k^2 w_0^2},\ b_1 = -\frac{8\pi v_1 w_0^2}{k},\ c_1 = w_0^2 \tag{29}$$

$$a_2 = \frac{(16\pi v_2^2 T_0^4 + 1)\beta_2^2}{T_0^2},\ b_1 = -8\pi v_2 T_0^2 \beta_2,\ c_1 = T_0^2 \tag{30}$$

From Equations (27) and (28) we see that $w^2(z)$ and $T^2(z)$ are quadratic functions of z, and will reach minima when $z_1 = -b_1/2a_1$ and $z_2 = -b_2/2a_2$, respectively, i.e., the intensity maximum appears at distances:

$$z_{1,\min} = \frac{4\pi k v_1 w_0^4}{16\pi^2 v_1^2 w_0^4 + 1}, \tag{31}$$

$$z_{2,\min} = \frac{4\pi v_2 T_0^4}{(16\pi^2 v_2^2 T_0^4 + 1)\beta_2}, \tag{32}$$

where $z_{1,\min}$ depends on the v_1 and incident beam width w_0. $z_{1,\min}$ has an internal relationship with spatial coherence length σ by the rect weight function $p_{\mathrm{R}}(v_1)$ shown in Equation (5), while $z_{2,\min}$ depends on the v_2 and the pulse duration. And, $z_{2,\min}$ is in connection with temporal coherence length T_{c} by the rect weight function $p_{\mathrm{T}}(v_2)$ shown in Equation (6). Hence, when the self-focusing takes place at spatial and temporal dimensions simultaneously, the relationship between spatial parameters and temporal parameters can be obtained as follows:

$$\frac{k v_1 w_0^4}{16\pi^2 v_1^2 w_0^4 + 1} = \frac{v_2 T_0^4}{(16\pi^2 v_2^2 T_0^4 + 1)\beta_2}. \tag{33}$$

After a comparison between rect weight function and Gaussian weight function, it was seen that the intensity profiles of PCP beams with rect weight function are similar to the case of Gaussian weight function. However, specifically, the spatial-temporal self-focusing effect of the latter is more noticeable and the focal spot is much small—the value of peak intensity can reach 17.4 for the Gaussian weight function case. Nevertheless, the value is 9.3 for the rect weight function. In addition, the positions of focal spots where self-focusing in the spatial and temporal dimensions takes place simultaneously are different from each other. The positions of focal spot are z = 0.2 km and z = 0.04 km for the rect weight function and Gaussian weight function, respectively. That is to say, the spatial-temporal self-focusing effect of the latter takes place more early.

3.2. Air Case

In the following calculation, we present the evolution behavior of PCP beams in air medium. Because the refractive index n_{g} = 1.00028 of air is much closer to the 1, and the second-order dispersion coefficient β_2 = 0.021233 ps^2 km^{-1} is very small. Hence, we choose more short pulse duration and

temporal coherence length, namely, T_0 = 200 fs and T_c = 100 fs in order to present the self-focusing more clearly. The other parameters are the same as the case of water.

Figures 7 and 8 give the contour graph of normalized spatial-temporal intensity distribution $I(x, t, z)$ of PCP beams at z plane with different values of z. Figure 7 is the case of rect weight function, while Figure 8 is the case of Gaussian weight function. From Figures 7 and 8, we can see that the similar spatial-temporal self-focusing phenomenon takes place, i.e., the pulses focus first on the temporal dimension, then focus on the spatial dimension with increasing propagation distance z. At some critical distance, the spatial-temporal self-focusing phenomenon takes place (see Figure 7c z = 0.13 km and Figure 8c z = 0.04 km). Compared with rect weight function, for the case of Gaussian weight function, the spatial-temporal self-focusing behavior appears more early and noticeable. Physically, Gaussian weight function compared with rect weight function has better energy focusability.

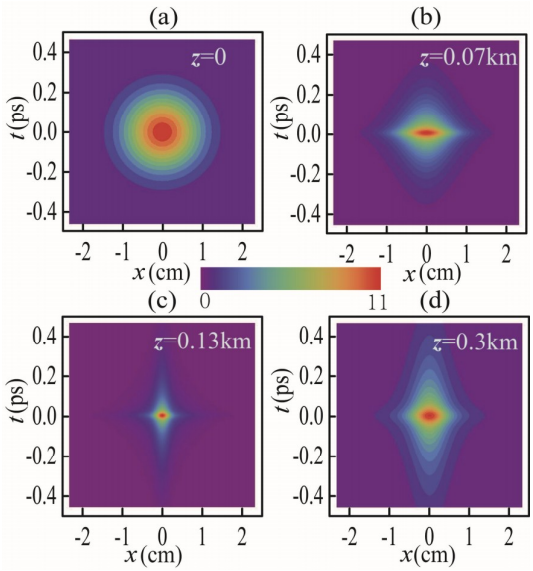

Figure 7. Contour graph of normalized spatial-temporal intensity distribution $I(x, t, z)$ of PCP beams with rect weight function at z plane with different values of z: (**a**) z = 0, (**b**) z = 0.07 km, (**c**) z = 0.13 km and (**d**) z = 0.3 km in the x-t plane.

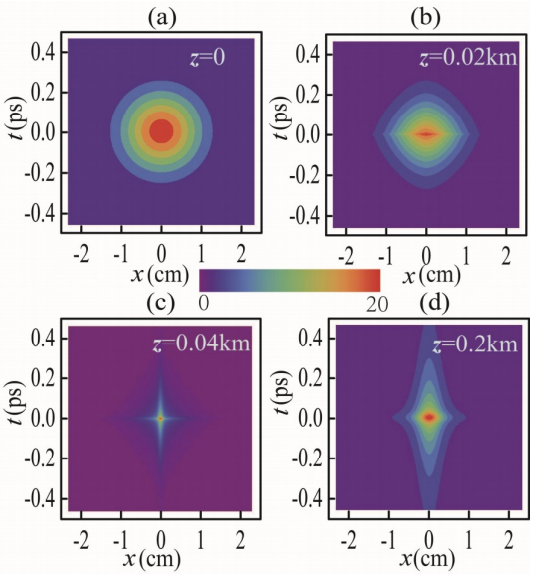

Figure 8. Contour graph of normalized spatial-temporal intensity distribution $I(x, t, z)$ of PCP beams with Gaussian weight function at z plane with different values of z: (**a**) z = 0, (**b**) z = 0.02 km, (**c**) z = 0.04 km and (**d**) z = 0.2 km in the x-t plane.

Figure 9 gives the on-axis and off-axis normalized intensity profile of PCP beams in air for the rect weight function (a,b) and Gaussian weight function (c,d), respectively. In general, the similar self-focusing phenomenon can be found for the rect weight function and Gaussian weight function of PCP beams. What is more, the self-focusing effect of PCP beams with Gaussian weight function is more noticeable than the case of rect weight function. Mathematically, there are high degrees of resemblance between rect function and Gaussian function. Physically, Gaussian weight function has better energy focusability than rect weight function.

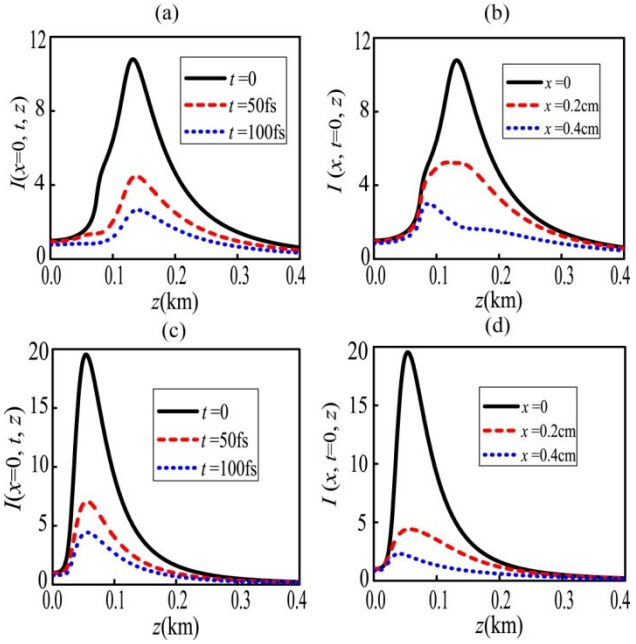

Figure 9. On-axis and off-axis normalized spatial-temporal intensity profile $I(x, t, z)$ of PCP beams at z plane with different values of t (**a**,**c**) and x (**b**,**d**).

4. Conclusions

In the present work, a novel class of spatially and temporally PCP source with circular spatial and sinc temporal coherence distribution is introduced. The evolution of pulsed beams generated by this kind of source in dispersive media is investigated. Water and air are chosen as two typical examples of dispersive medium. It is found that the pulsed beams exhibit spatial-temporal self-focusing behavior upon water/air propagation. The relationship between spatial parameters and temporal parameters of pulsed beams is acquired, where self-focusing takes place at spatial and temporal dimension simultaneously. A detailed comparison between the pulsed beams and the normal non-uniformly correlated PCP beams is performed. The results show that the spatial-temporal self-focusing phenomenon of non-uniformly correlated PCP beams with Gaussian weight function is more noticeable, and takes place more early. The results obtained can have potential applications in laser micromachining and laser filamentation [65]. For example, in laser micromachining, a proposed pulsed source might be generated in order to obtain a self-focusing spot upon propagation, where a suitable peak intensity is adopted to ablate the proposed material. In the process of micromachining, the profile of the focal spot can be modulated to improve fabrication resolution. In addition, in the field of laser filamentation, the intensity inside the filament can be enhanced by manipulating the mutual coherent function (MCF) of proposed pulsed source using a Spatial Light Modulater (SLM).

Author Contributions: Z.Z. Data Curation, writing-original draft, writing-review and editing; C.D. formal analysis, methodology; Y.Z. formal analysis; L.P. project administration. All authors read and approved the final manuscript.

Funding: This research was funded by the National Natural Science Foundation of China, grant numbers 61575091 and 61675094.

Conflicts of Interest: The authors declare no conflict of interest.

References

1. Mandel, L.; Wolf, E. *Optical Coherence and Quantum Optics*; Cambridge University: Cambridge, UK, 1995.
2. Wolf, E. *Introduction to the Theory of Coherence and Polarization of Light*, 1st ed.; Cambridge University Press: Cambridge, UK, 2007.
3. Gbur, G.; Visser, T.D. Can spatial coherence effects produce a local minimum of intensity at focus? *Opt. Lett.* **2003**, *28*, 1627–1629. [CrossRef]
4. Pu, J.; Nemoto, S.; Liu, X. Beam shaping of focused partially coherent beams by use of the spatial coherence effect. *Appl. Opt.* **2004**, *43*, 5281–5286. [CrossRef]
5. Van Dijk, T.; Fischer, D.G.; Visser, T.D.; Wolf, E. Effects of Spatial Coherence on the Angular Distribution of Radiant Intensity Generated by Scattering on a Sphere. *Phys. Rev. Lett.* **2010**, *104*, 173902. [CrossRef]
6. Sahin, S.; Korotkova, O. Light sources generating far fields with tunable flat profiles. *Opt. Lett.* **2012**, *37*, 2970–2972. [CrossRef]
7. Mei, Z.; Korotkova, O. Random sources generating ring-shaped beams. *Opt. Lett.* **2013**, *38*, 91–93. [CrossRef]
8. Cai, Y.; Chen, Y.; Wang, F. Generation and propagation of partially coherent beams with nonconventional correlation functions: A review. *J. Opt. Soc. Am. A* **2014**, *31*, 2083–2096, (invited). [CrossRef]
9. Cai, Y.; Chen, Y.; Yu, J.; Liu, X.; Liu, L. Generation of Partially Coherent Beams. In *Progress in Optics*; Elsevier BV: Amsterdam, The Netherlands, 2017; Volume 62, pp. 157–223.
10. Korotkova, O. Random sources for rectangular far fields. *Opt. Lett.* **2014**, *39*, 64–67. [CrossRef]
11. Li, J.; Wang, F.; Korotkova, O. Random sources for cusped beams. *Opt. Express* **2016**, *24*, 17779–17791. [CrossRef]
12. Wang, F.; Korotkova, O. Random sources for beams with azimuthal intensity variation. *Opt. Lett.* **2016**, *41*, 516–519. [CrossRef]
13. Mei, Z.; Korotkova, O. Random sources for rotating spectral densities. *Opt. Lett.* **2017**, *42*, 255–258. [CrossRef]
14. Reddy, S.G.; Kumar, A.; Prabhakar, S.; Singh, R.P. Experimental generation of ring-shaped beams with random sources. *Opt. Lett.* **2013**, *38*, 4441–4444. [CrossRef]
15. Wang, F.; Liang, C.; Yuan, Y.; Cai, Y. Generalized multi-Gaussian correlated Schell-model beam: From theory to experiment. *Opt. Express* **2014**, *22*, 23456–23464. [CrossRef]
16. Chen, Y.; Liu, L.; Wang, F.; Zhao, C.; Cai, Y. Elliptical Laguerre-Gaussian correlated Schell-model beam. *Opt. Express* **2014**, *22*, 13975–13987. [CrossRef]
17. Liang, C.; Wang, F.; Liu, X.; Cai, Y.; Korotkova, O. Experimental generation of cosine-Gaussian-correlated Schell-model beams with rectangular symmetry. *Opt. Lett.* **2014**, *39*, 769–772. [CrossRef]
18. Chen, Y.; Wang, F.; Liu, L.; Zhao, C.; Cai, Y.; Korotkova, O. Generation and propagation of a partially coherent vector beam with special correlation functions. *Phys. Rev. A* **2014**, *89*, 013801. [CrossRef]
19. Chen, Y.; Wang, F.; Zhao, C.; Cai, Y. Experimental demonstration of a Laguerre-Gaussian correlated Schell-model vortex beam. *Opt. Express* **2014**, *22*, 5826–5838. [CrossRef]
20. Iv, M.W.H.; Basu, S.; Xiao, X.; Voelz, D.G. Producing any desired far-field mean irradiance pattern using a partially-coherent Schell-model source. *J. Opt.* **2015**, *17*, 055607.
21. Milo, W.H.I.V.; Santasri, B.; David, G.V.; Xifeng, X. Experimentally generating any desired partially coherent Schell-model source using phase-only control. *J. Appl. Phys.* **2015**, *118*, 093102.
22. Chen, Y.; Gu, J.; Wang, F.; Cai, Y. Self-splitting properties of a Hermite-Gaussian correlated Schell-model beam. *Phys. Rev. A* **2015**, *91*, 013823. [CrossRef]
23. Chen, Y.H.; Ponomarenko, A.S.; Cai, Y.J. Experimental generation of optical coherence lattices. *Appl. Phys. Lett.* **2016**, *109*, 061107. [CrossRef]
24. Hyde, M.W.; Bose-Pillai, S.; Voelz, D.G.; Xiao, X. Generation of Vector Partially Coherent Optical Sources Using Phase-Only Spatial Light Modulators. *Phys. Rev. Appl.* **2016**, *6*, 064030. [CrossRef]
25. Chen, Y.; Ponomarenko, S.A.; Cai, Y. Self-steering partially coherent beams. *Sci. Rep.* **2017**, *7*, 39957. [CrossRef] [PubMed]

26. Hyde IV, M.W.; Bose-Pillai, S.; Voelz, D.G.; Xiao, X. A fast and efficient method for producing partially coherent sources. *J. Opt.* **2017**, *19*, 025601. [CrossRef]
27. Hyde, M.W.; Bose-Pillai, S.R.; Wood, R.A. Synthesis of non-uniformly correlated partially coherent sources using a deformable mirror. *Appl. Phys. Lett.* **2017**, *111*, 101106. [CrossRef]
28. Wan, L.P.; Zhao, D.M. Optical coherence grids and their propagation characteristics. *Opt. Express* **2018**, *26*, 2168–2180. [CrossRef] [PubMed]
29. Lin, H.; Zhou, X.; Chen, Z.; Sasaki, O.; Li, Y.; Pu, J. Tight focusing properties of a circular partially coherent Gaussian beam. *J. Opt. Soc. Am. A* **2018**, *35*, 1974–1980. [CrossRef] [PubMed]
30. Yu, J.; Cai, Y.; Gbur, G. Rectangular Hermite non-uniformly correlated beams and its propagation properties. *Opt. Express* **2018**, *26*, 27894–27906. [CrossRef] [PubMed]
31. de Sande, J.C.G.; Martínez-Herrero, R.; Piquero, G.; Santarsiero, M.; Gori, F. Pseudo-Schell model sources. *Opt. Express* **2019**, *27*, 3963–3977. [CrossRef] [PubMed]
32. Liang, C.; Khosravi, R.; Liang, X.; Kacerovská, B.; Monfared, Y.E.; Khosrav, R. Standard and elegant higher-order Laguerre–Gaussian correlated Schell-model beams. *J. Opt.* **2019**, *21*, 085607. [CrossRef]
33. Wu, G.F.; Cai, Y.J. Detection of a semirough target in turbulent atmosphere by a partially coherent beam. *Opt. Lett.* **2011**, *36*, 1939–1941. [CrossRef]
34. Singh, M.; Lajunen, H.; Tervo, J.; Turunen, J. Imaging with partially coherent light: Elementary-field approach. *Opt. Express* **2015**, *23*, 28132. [CrossRef] [PubMed]
35. Gbur, G. Partially coherent beam propagation in atmospheric turbulence. *J. Opt. Soc. Am. A* **2014**, *31*, 2038–2045, (invited). [CrossRef] [PubMed]
36. Santarsiero, M.; Martínez-Herrero, R.; Maluenda, D.; De Sande, J.C.G.; Piquero, G.; Gori, F. Partially coherent sources with circular coherence. *Opt. Lett.* **2017**, *42*, 1512–1515. [CrossRef] [PubMed]
37. Santarsiero, M.; Martínez-Herrero, R.; Maluenda, D.; De Sande, J.C.G.; Piquero, G.; Gori, F. Synthesis of circularly coherent sources. *Opt. Lett.* **2017**, *42*, 4115–4118. [CrossRef] [PubMed]
38. Iv, M.W.H.; Bose-Pillai, S.R. Partially coherent sources with circular coherence: Comment. *Opt. Lett.* **2017**, *42*, 3084.
39. Ding, C.; Koivurova, M.; Turunen, J.; Pan, L. Self-focusing of a partially coherent beam with circular coherence. *J. Opt. Soc. Am. A* **2017**, *34*, 1441–1447. [CrossRef]
40. Torres-Company, V.; Lancis, J.; Andrés, P. Incoherent frequency-to-time mapping: Application to incoherent pulse shaping. *J. Opt. Soc. Am. A* **2007**, *24*, 888–894. [CrossRef]
41. Agrawal, G.P. *Nonlinear Fiber Optics*, 4th ed.; Academic: New York, NY, USA, 2007.
42. Nan, S.; Bai, Y.; Shi, X.; Shen, Q.; Qu, L.; Li, H.; Fu, X. Experimental investigation of ghost imaging of reflective objects with different surface roughness. *Photonics Res.* **2017**, *5*, 372–376. [CrossRef]
43. Turunen, J. Low-Coherence Laser Beams. In *Laser Beam Propagation: Generation and Propagation of Customized Light*; Forbes, A., Ed.; CRC Press: Boca Raton, FL, USA, 2014.
44. Pääkkönen, P.; Turunen, J.; Vahimaa, P.; Friberg, A.T.; Wyrowski, F. Partially coherent Gaussian pulses. *Opt. Commun.* **2002**, *204*, 53–58. [CrossRef]
45. Wang, L.; Lin, Q.; Zhu, S. Partially coherent light pulse and its propagation. *Opt. Commun.* **2003**, *219*, 65–70.
46. Lajunen, H.; Tervo, J.; Vahimaa, P. Theory of spatially and spectrally partially coherent pulses. *J. Opt. Soc. Am. A* **2005**, *22*, 1536–1545. [CrossRef]
47. Lancis, J.; Torres-Company, V.; Silvestre, E.; Andrés, P. Space–time analogy for partially coherent plane-wave-type pulses. *Opt. Lett.* **2005**, *30*, 2973–2975. [CrossRef] [PubMed]
48. Torres-Company, V.; Mínguez-Vega, G.; Lancis, J.; Friberg, A.T. Controllable generation of partially coherent light pulses with direct space-to-time pulse shaper. *Opt. Lett.* **2007**, *32*, 1608–1610. [CrossRef] [PubMed]
49. Torres-Company, V.; Lajunen, H.; Lancis, J.; Friberg, A.T. Ghost interference with classical partially coherent light pulses. *Phys. Rev. A* **2008**, *77*, 043811. [CrossRef]
50. Ding, C.; Cai, Y.; Korotkova, O.; Zhang, Y.; Pan, L. Scattering-induced changes in the temporal coherence length and the pulse duration of a partially coherent plane-wave pulse. *Opt. Lett.* **2011**, *36*, 517–519. [CrossRef] [PubMed]
51. Mokhtarpour, L.; Ponomarenko, S.A. Complex area correlation theorem for statistical pulses in coherent linear absorbers. *Opt. Lett.* **2012**, *37*, 3498–3500. [CrossRef] [PubMed]
52. Dutta, R.; Korhonen, M.; Friberg, A.T.; Genty, G.; Turunen, J. Broadband spatiotemporal Gaussian Schell-model pulse trains. *J. Opt. Soc. Am. A* **2014**, *31*, 637–643. [CrossRef] [PubMed]

53. Dutta, R.; Friberg, A.T.; Genty, G.; Turunen, J. Two-time coherence of pulse trains and the integrated degree of temporal coherence. *J. Opt. Soc. Am. A* **2015**, *32*, 1631–1637. [CrossRef]
54. Dutta, R.; Turunen, J.; Friberg, A.T. Michelson's interferometer and the temporal coherence of pulse trains. *Opt. Lett.* **2015**, *40*, 166–169. [CrossRef]
55. Zhang, Y.; Ji, X.; Zhang, H.; Li, X.; Wang, T.; Wang, H.; Deng, Y. Self-focusing and group-velocity dispersion of pulsed laser beams in the inhomogeneous atmosphere. *Opt. Express* **2018**, *26*, 14617–14625. [CrossRef]
56. Lajunen, H.; Saastamoinen, T. Non-uniformly correlated partially coherent pulses. *Opt. Express* **2013**, *21*, 190–195. [CrossRef] [PubMed]
57. Ding, C.L.; Cai, Y.J.; Zhang, Y.T.; Wang, H.X.; Zhao, Z.G.; Pan, L.Z. Stochastic electromagnetic plane-wave pulse with non-uniform correlation distribution. *Phys. Lett. A* **2013**, *377*, 1563–1565. [CrossRef]
58. Ding, C.; Korotkova, O.; Pan, L. The control of pulse profiles with tunable temporal coherence. *Phys. Lett. A* **2014**, *378*, 1687–1690. [CrossRef]
59. Ding, C.; Korotkova, O.; Zhang, Y.; Pan, L. Cosine-Gaussian correlated Schell-model pulsed beams. *Opt. Express* **2014**, *22*, 931–942. [CrossRef] [PubMed]
60. Ding, C.; Koivurova, M.; Turunen, J.; Pan, L. Temporal self-splitting of optical pulses. *Phys. Rev. A* **2018**, *97*, 053838. [CrossRef]
61. Liu, X.Y.; Zhao, D.M.; Tian, K.H.; Pan, W.Q.; Zhang, K.W. Gaussian temporal modulation for the behavior of multi-sinc Schell-model pulses in dispersive media. *Opt. Commun.* **2018**, *416*, 160–165. [CrossRef]
62. Luo, M.L.; Zhao, D.M. Characterizing the polarization and cross-polarization of electromagnetic vortex pulses in the space-time and space-frequency domain. *Opt. Express* **2015**, *23*, 4153–4162. [CrossRef]
63. Lajunen, H.; Turunen, J.; Vahimaa, P.; Tervo, J.; Wyrowski, F. Spectrally partially coherent pulse trains in dispersive media. *Opt. Commun.* **2005**, *255*, 12–22. [CrossRef]
64. Lajunen, H.; Saastamoinen, T. Propagation characteristics of partially coherent beams with spatially varying correlations. *Opt. Lett.* **2011**, *36*, 4104–4106. [CrossRef]
65. Jing, C.; Qi, X.; Wang, Z.; Ma, B.; Ding, C. Comparative study of femtosecond filamentation properties in the classical model and the full model for different incident pulse durations. *J. Opt.* **2019**, *21*, 065503. [CrossRef]